JOURNAL OF CATALYSIS 141, 191–205 (1993)

Characterization and Ammonia Synthesis Activity of Ruthenium Zeolite Catalysts

MARK D. CISNEROS[1] AND JACK H. LUNSFORD[2]

Department of Chemistry, Texas A&M University, College Station, Texas 77843

Received September 28, 1992; revised December 11, 1992

Ruthenium metal in a series of alkali-metal-exchanged faujasite-type zeolites was found to be active for the catalytic synthesis of ammonia from dihydrogen and dinitrogen at temperatures between 300 and 450°C and at atmospheric pressure. A triply promoted iron catalyst exhibited a lower activity under similar conditions. Following reduction in hydrogen, the ruthenium metal crystallites were located within the pore structure of the zeolite microcrystals. Variation of the exchangeable alkali-metal cations and the silicon-to-aluminum ratio altered the activity of the ruthenium catalysts, with RuKX being the most active material. By applying Sanderson's electronegativity calculations to the ruthenium zeolites, a relationship was found between the turnover frequency for ammonia synthesis and the effective oxygen charge, which was a function of the cation and the Si/Al ratio. Presumably negative charge is transferred from the oxygen to the metal, thereby enhancing the rate of N_2 dissociation. The metal particle size also influenced the activity; larger particles were more active. A RuHY zeolite was the least active among the catalysts studied.

INTRODUCTION

The prevailing industrial ammonia synthesis process utilizes a triply promoted iron catalyst operating at temperatures between 400 and 700°C and at pressures in excess of 300 atm. These severe reaction conditions require tremendous energy input. Advances in engineering within the past 40 years have afforded a threefold decrease in the energy consumption per metric ton of ammonia produced (*1*). In recent years, catalyst modification to realize additional energy savings has not been a major industrial research focus; however, a marked improvement in the activity would allow one to operate at lower temperatures and, therefore, lower pressures. Ozaki and co-workers (*2*, *3*) in the early 1970s introduced an alkali-metal-promoted carbon-supported ruthenium catalyst (Ru/AC–M, where AC is activated carbon and M is an alkali metal) which exhibited a 10-fold increase in activity over the conventional iron catalyst under similar conditions. This novel catalyst has gained industrial attention as shown by plans for commercial usage (*4*).

With the introduction of the ruthenium-based materials as a superior ammonia synthesis catalyst, additional investigations were carried out to probe the effects of other supports and other electronic promoters. Aika and co-workers (*5*) have completed work on a large number of ruthenium-supported catalysts: the supports include MgO, BeO, and CaO, in addition to the activated carbon mentioned above. The effects of promoters and support suggest that the donation of electrons to the Ru is favorable for ammonia synthesis, which is consistent with the observation that N≡N bond breaking is the most difficult step in the cycle. The addition of electrons to the N_2 molecule, via the catalyst, facilitates the breaking of these bonds (*6*). The proximity of the promoter to the ruthenium metal and its interaction with the support are very important considera-

[1] Present address: The DOW Chemical Company Plaquemine, Louisiana 70765.

[2] To whom correspondence should be addressed.

0021-9517/93 $5.00

tions. Further investigations of these interactions could provide valuable insight into the structural and electronic promotion effects.

Zeolites offer an attractive system for studying the mode of interaction between promoters and metal particles because (i) the locations of the particles and alkali-metal cations are reasonably well defined, (ii) the metal is in intimate contact with the support through a three-dimensional network of oxygen ions, (iii) the nature of the cation can be easily modified, and (iv) the zeolite itself functions as the anion. Larsen and Haller (*7*) have taken advantage of these factors to interpret the interactions that occur between Pt clusters and their L-zeolite host. Both the amount of CO adsorbed on the Pt clusters and the ratio of toluene-to-benzene adsorption, as determined by kinetic measurements, decreased as the ionic radius-to-charge of the cation increased (i.e., Ba > Ca > Mg). It was suggested that the clusters interact electronically with the support, perhaps via charge transfer. Gallezot (*8*) had previously pointed out that small Pt or Pd particles in zeolites have unusual electronic properties which may involve electron transfer from the metal to the zeolite.

Bai and Sachtler (*9*) have reported a promotional effect of the exchangeable alkali-metal cations of a Pd/MY zeolite (M = Li, Na, K) on the conversion of methylcyclopentane. The activity for ring opening increased in the sequence $Li^+ < Na^+ < K^+$. They proposed that according to this sequence the alkali-metal cations lowered the acid strength of the zeolite protons, while electron transfer occurred from donor sites to the palladium metal particles. The donor sites were suggested to be the oxygen anions bound to aluminum cations within the zeolite lattice (*10*). Sachtler and co-workers (*11*) have also studied the conversion of neopentane over a Pd/NaHY catalyst. The reaction rate correlated well with the proton content of the catalyst. Moreover, the observed rate was two orders of magnitude greater than for a Pd/SiO_2 catalyst. The increase in the reaction rate was attributed to the formation of adducts of metal particles and protons, which react easily with a hydrocarbon.

Lunsford and co-workers (*12*, *13*) used a ruthenium-based zeolite catalyst to activate carbon monoxide for the methanation reaction. The ruthenium was dispersed in a Y-type faujasite, and the ruthenium metal particle size was on the order of 10–25 Å. The effect of the exchangeable alkali-metal cations within a RuY system was studied by Goodwin and co-workers (*14*), who used the CO hydrogenation reaction as a probe. Little effect on the activity and chain growth for CO hydrogenation was noted; however, dramatic changes in the secondary reactions of primary olefinic products were observed as the exchangeable cations were varied. Goodwin proposed that this behavior could result from possible modifications of the acid sites produced during reduction of the ruthenium.

Mahdi *et al.* (*15*) have recently reported that a ruthenium-exchanged NaY zeolite was active for ammonia synthesis at atmospheric pressure. The turnover frequency ($1.8 \times 10^{-4} s^{-1}$) remained constant at 420°C for up to 70 h, but at 540°C the activity of the catalyst decreased with time. The long-term deactivation was found to be reversible by a controlled oxidative treatment. The activity is attributed to cluster-like Ru metal particles.

The following study demonstrates that the type of cation, as well as the Si/Al ratio has a marked effect on the ammonia synthesis activity of Ru containing zeolites. Other factors such as the size of the Ru particles and the location of the Ru, either within the zeolite crystals or external to the crystals also were investigated. Although the primary purpose of the research was to determine the importance of these variables on the rate of ammonia formation, the sensitivity of this reaction to electronic effects makes it an ideal probe to study metal–support interactions.

EXPERIMENTAL

Catalysis

High-purity NaX and NaY zeolites obtained from Union Carbide were used as starting materials. The zeolite X had a silicon-to-aluminum ratio of 1.5 as characterized by X-ray diffraction and elemental analysis; the number of aluminum atoms per unit cell was 76. The Y-type zeolite had a silicon-to-aluminum ratio of 2.4, which corresponded to 56 Al/u.c. The sodium zeolites were ion exchanged at 40°C three times with the appropriate alkali-metal nitrate using 10 g of zeolite and 2 liters of 0.1 *M* aqueous solution. The material was suction filtered and air dried. An aqueous solution with 0.312 g of $Ru(NH_3)_6Cl_3$ (Aldrich) was used to ion-exchange at 40°C 5 g of the alkali-metal zeolite. Ninety-eight percent of the ruthenium was removed from the solution by ion exchange, which resulted in a zeolite with a 2 wt% ruthenium metal loading. After the latter ion-exchange, the ruthenium-alkali-metal zeolite was suction filtered and washed three times with 1 liter aliquots of distilled-deionized water in order to remove all counter ions such as nitrate and chloride. This material was air dried and seived to 20–42 mesh.

A RuKX catalyst also was prepared by dehydrating a KX zeolite ($62K^+$/u.c.) under vacuum and adding $Ru_3(CO)_{12}$. The solid mixture was sealed in a vial and placed in an oven at 80°C for 20 days. All of the ruthenium carbonyl was assumed to sublime into the zeolite. The ruthenium metal loading was nominally 2 wt%. The catalyst was used without exposure to air.

A 1g sample of catalyst was loaded into a Pyrex plug-flow straight tube reactor. Quartz chips were placed above the catalyst bed to ensure gas preheating. The standard pretreatment involved heating the material *in vacuo* for 1-h periods at temperatures of 100, 200, 300, and 450°C. The reactor was cooled, and ultra-high-purity hydrogen (Matheson) was admitted through an oxygen and water scrubber assembly. The scrubber assembly contained 10% Na/Al_2O_3 and 5% MnO/SiO_2. The hydrogen flow was regulated with a mass flow controller at a flow rate of 150 $cm^3\ min^{-1}$ while the temperature was ramped (30°C min^{-1}) to 450°C. The relatively high flow rate allowed the water formed during reduction to be removed quickly from the catalyst. The reduction was continued at 450°C for 2 h, and after the reactor was cooled *in vacuo*, activity studies were carried out. The reduction of the ruthenium metal approached 100% as determined by temperature-programmed reduction. The catalytic activity remained stable over the 4–6 h period during which it was measured.

A triply promoted iron catalyst was obtained from UCI Catalysts. Four grams of the catalyst was loaded into the reactor. The prescribed activation treatment as suggested by the manufacturer was followed. Hydrogen was admitted at a flow rate of 150 $cm^3\ min^{-1}$, and the temperature of the catalyst was increased slowly from 25 to 360°C over a 4-day period. The temperature of the catalyst was held constant at 360°C for 2 days under flowing hydrogen. Subsequently, the temperature was increased slowly (over a 2-day period) to 450°C. The catalyst was cooled under flowing hydrogen. Activity studies followed.

A gas mixture (Matheson) of H_2 and N_2 (typically 3 : 1) was passed through the reactor at a flow rate of 75 $cm^3\ min^{-1}$, which corresponds to a space velocity of 1500 h^{-1}. The catalyst bed temperature was increased to 300°C, and the temperature profile for ammonia synthesis activity was measured up to 450°C. Routinely, at least 15 min were allowed for the system to reach equilibrium before activity measurements were taken.

To detect the small amount of ammonia (as low as 100 ppb) in the effluent gas, a difference in conductivity was measured. In principle, the ammonia reacts with the available protons within the dilute sulfuric acid solution, and a change in the conductivity results. The detection system included a conductivity meter, a voltage multiplier, a

digital voltmeter, and a chart recorder. The signal from the conductivity meter was multiplied by 10, and the resulting voltage was read on a digital voltmeter. The effluent gas was bubbled through a dilute sulfuric acid solution (one drop of concentrated sulfuric acid per 2 liter of distilled-deionized water) which was maintained at a constant temperature by continuous air flow. The solution was vigorously stirred. A difference in conductivity was measured as a function of time. This measurement yielded the concentration of ammonia per unit time. The system was calibrated by using the ammonia that was evolved from an NH_4Y zeolite as it was heated to 450°C.

Elemental Analysis

Typically, 0.1 g of catalyst was placed in a Teflon beaker. The catalyst was mixed with 5 ml of distilled-deionized water, 2 ml of sulfuric acid, and at least 5 ml of hydrofluoric acid. The mixture was heated on a hot plate to dryness. After cooling, approximately 10 ml of a 10% hydrochloric acid solution was added and heated until the solid dissolved. Distilled-deionized water was added until 100 ml of solution was obtained. ICP spectroscopy was used to determine the bulk compositions of each catalyst sample. The amounts of ruthenium, aluminum, sodium, potassium, and cesium typically were determined in the respective zeolites. Silicon could not be analyzed using this method due to the formation of volatile silicon tetrafluoride during the dissolution process.

Hydrogen Chemisorption

Conventional volumetric gas expansion was employed to measure the amount of hydrogen chemisorbed on the ruthenium metal crystallites. Approximately 0.25 g of fresh catalyst was loaded into a flow-through Pyrex U-tube reactor. The samples were heated under vacuum to remove the zeolitic water. The temperature was increased to 100, 200, 300, and 450°C; the sample was maintained at each temperature for 1 h. After dehydration up to 450°C, the sample was cooled under vacuum. Ultra-high-purity H_2 was admitted at a flow rate of 150 $cm^3\ min^{-1}$, and the temperature was ramped to 450°C. The reduction of the catalyst was nominally for 2 h. After the material was reduced at 450°C, the catalyst was placed *in vacuo* at the elevated temperature for 1 h to remove any chemisorbed hydrogen. After cooling, hydrogen chemisorption isotherms were measured at room temperature. An equilibration time of 30 min was allowed for each datum point.

Temperature-Programmed Reduction/ Desorption

The extents of reduction and dispersion of ruthenium metal were studied using a temperature programmed reduction/desorption (TPR/TPD) apparatus. A 60-mg sample of RuKX was loaded into a quartz U-tube reactor, and a plug of sodium carbonate was loaded into the reactor exit to neutralize any acid formation during decomposition. The ruthenium catalyst was dehydrated under flowing helium at a rate of 12 $cm^3\ min^{-1}$, which corresponded to a space velocity of 3000 h^{-1}. The temperature was increased at a rate of 2°C min^{-1}, from 25 to 490°C, and the reactor subsequently was cooled under flowing helium. At room temperature, a 5% H_2/N_2 gas mixture was admitted at a flow rate of 12 $cm^3\ min^{-1}$. A dry ice/acetone bath was placed around a U-tube trap at the reactor exit in order to freeze out any water produced during the reduction process. The temperature of the reactor was increased at a rate of 20°C min^{-1} from 25°C to 400°C. Hydrogen consumption was measured as a function of temperature using a thermal conductivity detector (TCD).

The dispersion of the metal, which is the fraction of metal atoms at the surface of a particle, was determined from the hydrogen which chemisorbed on the ruthenium metal crystallites after the reduction process. After the TPR traces has been obtained, the sample was cooled under a flowing mixture of 5% hydrogen in nitrogen. At room tem-

perature the flow was changed to pure N_2 at 12 cm^3 min^{-1}, the temperature was ramped at a rate of 20°C min^{-1}, and the desorption of hydrogen was measured with the TCD.

Transmission Electron Microscopy

Low- and high-magnification micrographs of the zeolite crystallites were obtained with a Philips EM400T transmission electron microscope at an accelerating potential of 120 kV. The catalysts were exposed to air and ground into a powder. The powder was dusted onto a 3-mm-diameter carbon-coated *holey* copper grid. The microscope magnification was calibrated against an asbestos fiber lattice spacing and a diffraction grating replica (Ted Pella Inc.) to insure accurate measurements of the ruthenium metal crystallites. Energy dispersive X-ray analysis (EDX) was performed with the grid tilted 22° toward the X-ray detector. The electron beam spot size approached 25 mm in diameter during the EDX analysis.

X-ray Photoelectron Spectroscopy

After pretreatment in the catalytic reactor, the used catalyst was isolated from the vacuum line and placed into a glove box containing nitrogen. The catalyst powder was pressed into a small pellet (7 mm diameter, 1 mm thick) and placed onto a flat gold-coated copper sample holder. The sample assembly was loaded into a probe, located within the glove box, for insertion into the XPS instrument.

A Hewlett Packard 5950A ESCA Spectrometer was used to obtain the X-ray photoelectron spectra. The system is differentially pumped; therefore, the samples were inserted slowly into the analyzer chamber where a pressure $< 5 \times 10^{-8}$ Torr was maintained. Monochromatic X-rays were produced at an energy of 1487 eV (Al$K\alpha$) and at a power of 800 W. Since the zeolite sample is an insulating material, a flood gun was used for charge compensation. The Ru 3*d*, Na 2*p*, K 2*p*, Al 2*p*, Si 2*p*, and C 1*s* peaks were typically monitored. The C 1*s* peak at 284.6 eV was used as a reference for binding energy shifts.

Fourier Transform Infrared Spectroscopy

The catalyst powder was dusted onto a polished stainless steel die, and a thin wafer of uniform thickness was formed at pressures up to 3400 kg cm^{-2}. A flow-through quartz cell allowed a similar pretreatment schedule to that used in the pretreatment for the catalytic reaction. The sample wafer was raised into the heated region and dehydrated up to 450°C, followed by reduction for 2 h in H_2. The wafer was quickly lowered into the room temperature region of the cell, and the infrared spectrum was monitored between 4400 and 400 wavenumbers using a Fourier transform infrared spectrometer with a cryogenic mercury–cadmium–tellurium detector. The spectra were typically obtained at a resolution of 8 cm^{-1} after 256 accumulations.

RESULTS AND DISCUSSION

Crystallinity

The crystallinity of the zeolite-X catalysts was monitored before and after reaction. The (111) and (533) reflections were used as a measure of crystallinity. Breck (*16*) used a similar technique to monitor the crystallinity of NaX after steaming. Gustafson (*17*) has shown that RuY maintains crystallinity upon reduction up to 380°C.

The KX zeolite before reaction was assumed to be 100% crystalline. Upon ion-exchange with ruthenium, the material appeared to lose about 50% of its crystallinity; however, after reaction, the RuKX appeared to gain crystallinity. The other ruthenium-alkali-metal zeolite-X catalysts behaved in a similar fashion. This apparent loss in crystallinity may be an artifact, as the changes in the relative x-ray intensities result from the absorption of X-rays by the high-molecular-weight ions within the zeolite. Hathaway and Davis (*18*) noted a similar problem in alkali-metal-exchanged zeolite X. Instead of X-ray diffraction, pore volume measurements were used to deter-

TABLE 1

Elemental Composition of Catalysts

Catalyst	Elemental composition[a]
RuNaX	$Ru_{3.5}Na_{57}H_{19}[(AlO_2)_{76}(SiO_2)_{116}]$
RuKX	$Ru_{3.5}Na_7K_{55}H_{14}[(AlO_2)_{76}(SiO_2)_{116}]$
RuNaKX	$Ru_{3.5}Na_{20}K_{38}H_{18}[(AlO_2)_{76}(SiO_2)_{116}]$
RuCsX	$Ru_{3.5}Na_7Cs_{22}H_{47}[(AlO_2)_{76}(SiO_2)_{116}]$
RuKY	$Ru_{3.5}Na_2K_{36}H_{18}[(AlO_2)_{56}(SiO_2)_{136}]$
RuHY	$Ru_{3.5}Na_5H_{51}[(AlO_2)_{56}(SiO_2)_{136}]$

[a] The number of protons is based on the required charge compensation, assuming no dehydroxylation or dealumination.

mine crystallinity. Using this technique, they showed that a KX under thermal treatment up to 350°C only lost 4% of its crystallinity, and a CsX lost 16% of its crystallinity.

In order to obtain an acidic RuHX zeolite that contained a minimum number of alkali metal ions, a $RuNH_4X$ zeolite was prepared. Upon decomposition and under reaction conditions, the formation of RuHX was presumed. The crystallinity of the RuHX was tested by X-ray diffraction before and after reaction in a powder diffraction cell which could be isolated from the atmosphere. No reflections were observed in the diffractogram for the RuHX after reaction; all crystallinity was lost. A similar occurrence was noted by Kuhl and Schweizer (*19*). The thermal stability of NaHX zeolite increased as the number of sodiums per unit cell increased. To obtain a zeolitic material with a small concentration of alkali-metal cations, the more stable Y-type zeolite was used.

Variation in Composition

The compositions of the catalysts used in this study, with their designations, are shown in Table 1. The Na^+ cations were exchanged with K^+, Cs^+, or NH_4^+ cations, or combinations of these. Potassium exchange was relatively complete, yielding an ion-exchange level of 92%, while in the case of cesium exchange, the extent of ion exchange was only 39%. Similar results were observed by Garces *et al.* (*20*) when a NaX material was exchanged with alkali-metal ions. Using alkali-metal nitrate or hydroxide solutions for aqueous ion exchange, the extent of exchange for K^+ was 88% and for Cs^+ was 39%. Hathaway and Davis (*18*) reported a 51% exchange of Cs^+ for Na^+; however, the zeolite was impregnated with CsOH and not rinsed. The decrease in the extent of ion exchange with $Na^+ > K^+ > Cs^+$ in zeolite X has been explained by steric and other considerations (*21, 22*).

Even when there was no intent to introduce protons in to the zeolite (e.g., RuNaX) the balancing of charge requires that some be present. The reduction of Ru^{3+} may account for 10 H^+/u.c. In the compositions of Table 1 the number of protons were determined by difference; however, the infrared results indicate that the number of protons may be less than indicated (see below).

Direct Particle Size Measurement

Transmission electron microscopy (TEM) was used to directly image and measure the ruthenium metal crystallites. The micrograph of a RuKX zeolite prepared by the standard treatment is shown in Fig. 1a. A uniform distribution of ruthenium metal particles was observed for the catalyst. The ruthenium metal particle size ranged from 7–25 Å (±5 Å). A summary of the results for this and other zeolite catalysts is given in Table 2. The size of the ruthenium crystallites of all the catalysts was between 5 and 26 Å. The electron micrograph image confirms that the ruthenium particles were uniformly dispersed throughout the zeolite. Energy dispersive X-ray analysis (EDX),

FIG. 1. (a) Transmission electron micrograph of an internal RuKX catalyst. Magnification 433,333×. (b) Transmission electron micrograph of an external RuKX catalyst. Magnification 47,000×.

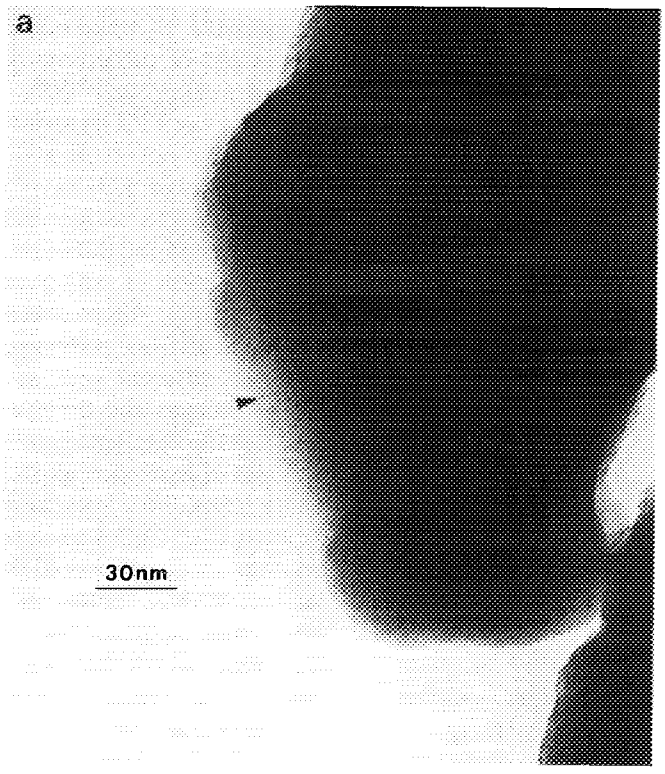
a
30nm

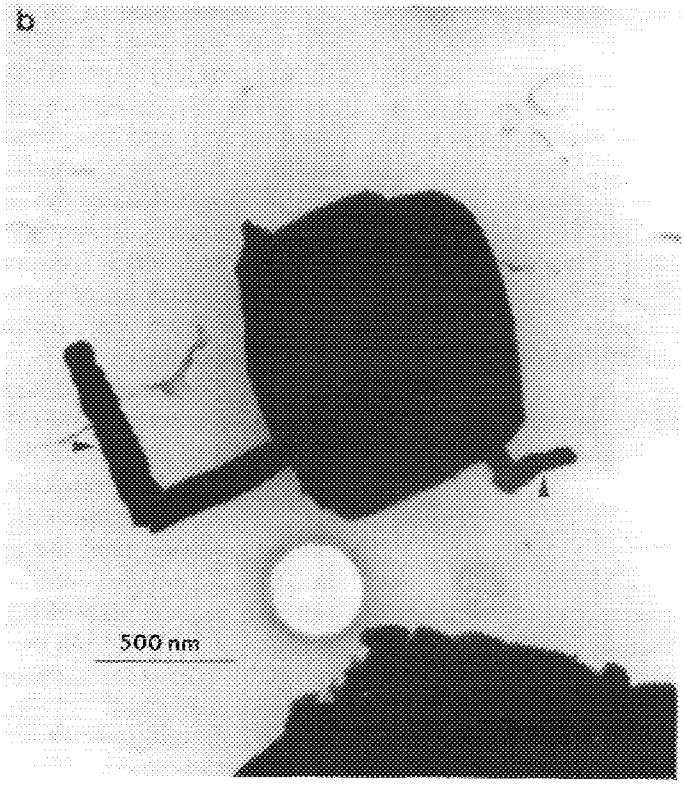
b
500 nm

TABLE 2

Ruthenium Particle Size and Dispersion

Catalyst	From TEM	H_2 chemisorption	
	d(Å)	D_h(%)	d(Å)
RuNaX	8–24	90	10
RuNaX[a]	—	40	29
RuKX	7–25	80	16
RuCsX	5–16	61	20
RuKY	10–20	64	19
RuHY	7–26	41	29

[a] Sample reduced at an H_2 flow rate of 14 cm^3 min^{-1}.

using an electron beam spot size approaching 25 nm, confirmed the presence of ruthenium.

A second type of catalyst was prepared in which the ruthenium was largely external to the zeolite. Verdonck *et al.* (*23*) and Pedersen and Lunsford (*24*) have reported that ruthenium migrates to the external surface of a zeolite when exposed to oxygen at temperatures as low as 250°C. In the present study a RuKX catalyst was heated in flowing O_2 for 1 h at 450°C and then was reduced as indicated previously. As shown in the electron micrograph of Fig. 1b, large ruthenium pillars grow on the external surfaces of the zeolite crystals. Upon greater magnification it is evident that the pillars are polycrystalline. The pillars grew to a height of several thousand Å above the surface and they often turned at right angles. EDX data confirmed that the pillars were mainly composed of ruthenium. These catalysts will be referred to as having external Ru; unless stated otherwise it is intended that the Ru is located within the zeolite cavities.

Indirect Particle Size Measurement

Temperature-programmed reduction and desorption were used to examine indirectly the ruthenium crystallites of the RuKX catalyst. A RuKX catalyst was reduced in flowing H_2 up to 450°C; moreover, the temperature of the material was increased to 490°C to monitor any additional H_2 uptake. No appreciable H_2 uptake was observed; thus the extent of ruthenium reduction was assumed to approach 100%.

During the TPR experiment well resolved peaks were observed at 130 and at 400°C. Verdonck *et al.* (*23*) have attributed the different peaks to surface reduction at lower temperatures and diffusion of hydrogen into and reduction of bulk ruthenium at higher temperatures. Alternatively, the two peaks could arise from reduction of Ru ions located at different sites in the zeolite, e.g., in the α-cages and the β-cages.

After the catalysts had been reduced, the amount of hydrogen adsorbed on the ruthenium crystallites was measured. The total reduction of CuO was used to calibrate the system. A dispersion of 64% was obtained for the RuKX zeolite. A similar measurement was made on the external Ru and a dispersion of 8% was determined. These results for the RuKX catalysts are in reasonably good agreement with the TEM data and also with the hydrogen chemisorption data.

Hydrogen chemisorption in the static system also was used to determine the metal surface area and dispersion of Ru in the catalysts. The adsorption isotherm was extrapolated to zero pressure, which corresponds to the volume of a monolayer; this value was used to calculate the dispersion of the ruthenium metal. Assuming dissociative adsorption and 100% reduction, the "average" ruthenium metal particle size can be calculated from the amount of hydrogen chemisorbed (*25*).

The dispersion of the RuKX catalyst under reaction conditions was 80%, which corresponded to a 16-Å particle size. Dispersion and metal particle size measurements were obtained for most of the ruthenium zeolite catalysts, and the results are given in Table 2. All the catalysts exhibited an average particle size of ca. 10–30 Å. The agreement between the particle size determined by hydrogen chemisorption and TEM is reasonably good.

Goodwin and coworkers studied the effect of exchangeable alkali-metal cations on

the ruthenium particle size within zeolite Y (*26*). Using hydrogen chemisorption, some variation in the ruthenium particle size was observed, which was attributed to the ability of the zeolite to retain water. Variation in the alkali-metal cation changed the zeolitic water content. When the water is present during the reduction step, the metal particles sinter. Goodwin proposed that the metal sintering would be expected to decrease in the order LiY > NaY > KY > RbY > CsY; however, the strength of water retention within the zeolite was also related to the particle size of the ruthenium metal and the position of the particle within the zeolite structure. As the particle size increased, the strength of water retention decreased while water retention increased as the metal particles became more uniformly dispersed. These competing factors complicate the explanation of the exchangeable alkali-metal cation effect on the particle size.

As the exchangeable alkali-metal cations were changed from Na^+ and K^+, to Cs^+, the particle size for the ruthenium-zeolite-X catalysts increased. Changing from the X- to the Y-type zeolite also caused an increase in the ruthenium particle size. An increase in particle size was also noted in the RuHY, which is in agreement with Goodwin's results.

Several authors have noted that the size of the metal particles exceed the 13-Å diameter of the larger zeolite cavities. Gustafson and Lunsford (*12*) proposed that ruthenium crystallites in adjacent supercages are joined at the windows. Another explanation was proposed by Verdonck *et al.* (*23*), especially for the case of the RuHY. The HY system is particularly susceptible to hydrolysis of lattice aluminum caused by residual water. The hydrolysis of lattice aluminum causes defects in the zeolite structure, forming cracks and holes within the structure. If the ruthenium migrates into these defect areas, large ruthenium crystallites could form.

The chemisorption of H_2 on an industrial iron catalyst which had been reduced over a one week period was compared with chemisorption on the zeolite catalysts. The dispersion of the triply promoted iron catalyst was very low, ca. 0.3%. The low dispersion suggests the presence of a very large particle size, on the order of 300 nm. It may be, however, that smaller particles are present, but they are partially covered with promoters.

TABLE 3

XPS Results for Ruthenium Zeolites

Catalyst	Binding energy (eV)[a,b]			
	Si 2*p*	Ru $3d_{5/2}$	K $2p_{3/2}$	O 1*s*
RuKX	101.1	279.8	292.4	530.0
RuHY	102.2	280.5	—	531.4

[a] The peak positions are corrected with the C 1*s* peak adjusted to 284.6 eV.

[b] Error for binding energy measurement was ±0.4 eV.

Surface Characterization of Ruthenium Zeolite

X-ray photoelectron spectroscopy (XPS) was used to characterize the surface of selected ruthenium zeolite catalysts. The binding energies of several photoelectron peaks for RuKX and RuHY zeolites are shown in Table 3. The observation of a shift in the Si 2*p* binding energy with cation and type of zeolite is consistent with the results of Okamoto *et al.* (*27*). This suggests that the Si 2*p* line may not be a suitable internal reference in zeolites.

Although the binding energy of supported Ru is subject to final state effects which complicate the interpretation of the results, it is significant to note that the binding energy increased from 279.8 eV in RuKX to 280.5 eV in RuHY. This difference is consistent with the greater localization of charge on the metal in RuKX and the higher activity of this material in the ammonia synthesis reaction (see below). Hikita *et al.* (*28*) have

observed a similar binding energy shift from 280.8 eV in Raney Ru to 279.6 eV in potassium-promoted Raney Ru and have suggested that this difference may reflect electron transfer to the metal.

Acid Site Concentration

The Brønsted acid site concentration of various ruthenium zeolite catalysts was investigated with infrared spectroscopy. The areas of the 3646-cm^{-1} and the 3549-cm^{-1} peaks were used to monitor the formation of acid sites. As a limiting case Brønsted acid sites from an ammonium-Y zeolite was monitored by FTIR. Most of the Brønsted acid sites were formed when the NH_4Y zeolite reached 300°C, and the concentration attained a maximum at 400°C. A slight decrease in the area of the 3646-cm^{-1} and the 3549-cm^{-1} peaks above 400°C probably resulted from dehydroxylation of the zeolite.

Reaction of the synthesized ammonia with the acid sites was considered to be a possible explanation for the low measured activity of the RuHY catalyst (see below) as Brønsted acid sites were formed when a $RuNH_4Y$ catalyst was treated for 30 min at 350°C under a flowing hydrogen–nitrogen (3 : 1) gas mixture. Subsequent treatment under pure hydrogen for 30 min and under the hydrogen-nitrogen gas mixture for 17 h, however, did not perturb the Brønsted acid site concentration. Therefore, it was concluded that the synthesized ammonia did not react irreversibly with the zeolitic acid sites at 350°C.

The addition of potassium by ion-exchange into a $RuNH_4Y$ zeolite decreased the concentration of acid sites dramatically as shown by the results of Fig. 2. The areas of the hydroxyl peaks in RuKY decreased markedly as compared to those in RuHY. The concentration of Brønsted acid sites for the RuHY was calculated using the hydroxyl region of the HY zeolite as a reference. The HY zeolite contained 51 Brønsted acid sites per unit cell. By using the areas of the 3646-cm^{-1} and the 3549-cm^{-1} peaks, the RuHY was estimated to contain 42 acid

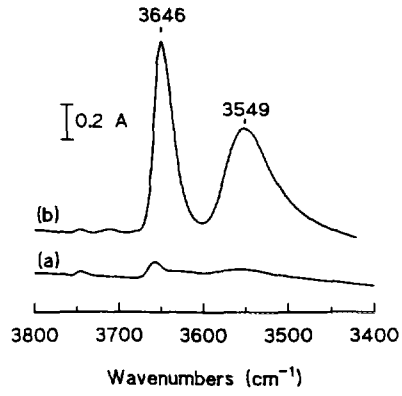

FIG. 2. Comparison of the hydroxyl region obtained by infrared spectroscopy of (a) RuKY catalyst and (b) RuHY catalyst.

sites per unit cell. The RuKY zeolite contained about 4 H^+/u.c. which is far less than the value of 18 H^+/u.c. reported in Table 1. This discrepancy is even more evident in the other alkali-metal zeolites. For example, almost no hydroxyl bands were detected in the RuKX zeolite, even though 14 H^+/u.c. are required to balance the charge. The low intensities of the OH bands could result from the interaction of the protons with the metal particles which would be expected to broaden the bands, perhaps beyond the limits of detection. It seems unlikely, however, that this would account for the absence of hydroxyl bands as the Ru particles fill only a small fraction of the supercages. More likely, during the preparation of the zeolites, particularly the X-type catalysts, there is dehydroxylation and perhaps a small amount of dealumination so that the amount of cations (i.e., protons) is less than the total amount of Al in the sample.

Catalytic Performance

It is evident from the results of Table 4 that a number of factors affect the activity of Ru-zeolites for ammonia synthesis including the type of cation, the Si/Al ratio and the metal particle size. The most active of the catalysts, both in terms of specific activity and turnover frequency (TOF) was the

TABLE 4

Activity of Ru-Zeolite Catalysts[a]

Catalyst	Activity × 10^4 (NH_3 molec s^{-1} Ru $atom^{-1}$)	TOF × 10^4 (s^{-1})	Activation energy (kcal/mol)
RuNaX	1.0	1.1	25
RuNaX[b]	2.8	6.9	25
RuKX	8.0	10	23
RuKX[c]	5.6	7.0	24
RuCsX	0.27	0.40	33
RuKY	0.44	0.69	28
RuHY	0[d]	—	—

[a] T = 350°C.
[b] Sample with 40% dispersion.
[c] Sample prepared from $Ru_3(CO)_{12}$.
[d] No measureable activity.

RuKX zeolite. The RuCsX zeolite was a factor of 15 less active at 350°C than the RuKX zeolite. This result is surprising as Ozaki and co-workers (*2*) found that the activity increased in the order Cs > K > Na for alkali-promoted ruthenium-based catalysts. The change in activity has been attributed to the decrease in the ionization potential which is in the order Na > K > Cs.

The RuKX catalyst prepared from $Ru_3(CO)_{12}$ had essentially the same activity over the temperature range from 305 to 450°C as did the analogous catalyst prepared from $Ru(NH_3)_6Cl_3$. This result suggests that the source of Ru is unimportant and in particular the presence of chlorine in the starting material does not influence the activity. It should be pointed out, however, that $RuCl_3$ is unsuitable as a reagent because with this compound Ru cannot be introduced into the zeolite.

Upon increasing the particle size by about a factor of 3 in the RuNaX zeolite, the activity more than doubled and the TOF increased by a factor of 4 over the entire temperature range tested. Dumesic *et al.* (*29*) noted a similar effect of the particle size on the turnover frequency for ammonia synthesis using Fe/MgO catalysts. As the dispersion of Fe decreased, the TOF increased. The increase of the TOF was attributed to the presence of C_7 sites which increased the rate of the ammonia synthesis reaction.

As an extreme case of particle growth one has the large Ru particles on the external surface of the zeolites. The activities of RuX catalysts with external Ru are compared with those of RuKX, RuNaX, and RuCsX zeolites in Fig. 3. The specific activity of the external Ru is much less, but, of course, the dispersion of this Ru is also less. Because of the large particle size, the error in the dispersion is large; however, it is estimated that the dispersion is about 2% from hydrogen adsorption data. This value is consistent with the size of the particles determined from the electron micrographs. Based upon this value the TOF at 400°C would be $18 \times 10^{-4}\ s^{-1}$, which is about half the value for the lower dispersion RuNaX zeolite.

From the data of Fig. 3 an apparent activation energy for ammonia synthesis over the RuKX zeolite was determined to be 22 ± 1 kcal mol^{-1} at a H_2/N_2 ratio of 3. At ratios of 2 and 1, the activation energies were 24 and 23 kcal mol^{-1}, respectively. Aika *et al.* (*5*) have reported values of 22 kcal mol^{-1} for

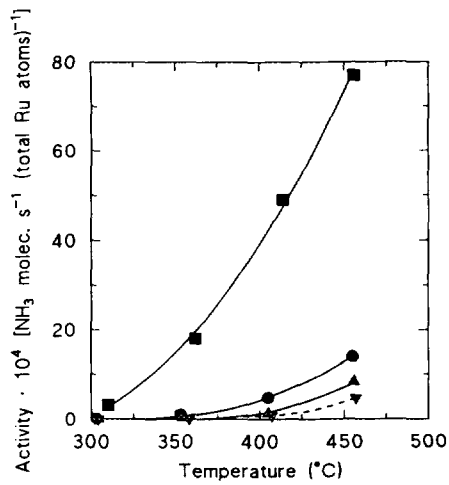

FIG. 3. Activity–temperature profile comparison of various RuX catalysts: (■) RuKX, (●) RuNaX, (▲) RuCsX, and (▼) all external RuX catalysts tested.

TABLE 5

Comparison of Turnover Frequencies of Various Ammonia Synthesis Catalysts

Catalyst	Dispersion (%)	TOF $s^{-1} \times 10^4$ (315°C)	Activity $\times 10^4$ (NH_3 molec s^{-1} Ru atom^{-1})
Ru/AC–K	10.3	205	21.1
Ru/BeO–K	8.6	204	17.5
Ru/MgO–K	2.9	197	5.7
Ru/Al_2O_3–K	5.0	100	5.0
Ru/CaO–K	2.5	74.7	1.9
Raney Ru–K	3.1	17.5	0.5
RuKX[b]	80	5.1	1.5

[a] All values, except where noted, were obtained from Ref (5).
[b] 304°C; this work.

the Ru/AC-K° catalyst, while a Ru–KOH/Al_2O_3 catalyst exhibited a value of 28 kcal mol^{-1}. The highly active Raney Ru catalyst promoted with Cs^+ had an E_a of only 19 kcal mol^{-1}.

The TOF at 310°C for the RuKX catalyst is compared in Table 5 with those reported by Aika *et al.* (*5*) for a number of ruthenium-based catalysts at 315°C. Clearly, the dispersion is greater and the TOF is less for the RuKX catalyst, although the TOF is comparable to that reported for the Raney Ru–K^0 catalyst. On the basis of activity per total amount of Ru atoms the RuKX zeolite compares much more favorably as a catalyst for ammonia synthesis. The latter comparison probably is more important for practical utilization because of the cost of ruthenium.

The specific activity of the RuKX catalyst was much greater than that of the industrial iron catalyst. For example, the activity of the RuKX catalyst at 407°C was 4.9×10^{-5} NH_3 molec. s^{-1} Ru atom^{-1} compared to a value of 1.2×10^{-5} NH_3 molec. s^{-1} Fe atoms^{-1} for the iron catalyst at the same temperature. This comparison is not entirely justified because the industrial catalyst was optimized for operation at higher temperatures and pressures. Nevertheless, Elofson and Gadallah (*30*) have shown that a ruthenium-based catalyst was superior to a triply promoted iron-based catalyst at elevated temperatures and pressures. At 400°C and 50 atm the ruthenium catalyst was more than twice as active as the iron catalyst.

Partial Oxygen Charge

The alkali-metal cations within the zeolite may promote the ammonia synthesis reaction in three ways: (i) by direct interaction with the metal particles, (ii) by a through-space interaction with the adsorbate or (iii) by modifying the electronic properties of the support. In the zeolite, many of the alkali-metal cations are in ion-exchanged sites removed from the metal, but the oxygen atoms of the support are in direct contact with the metal. In the following discussion, a model to determine the charge on the oxygen atoms of the zeolite is used to investigate the effect of the support on the ammonia synthesis reaction.

The Sanderson electronegativity equalization principle is an empirical method that allows one to determine the effective electronegativity of an atom within a molecule. Mortier (*31*) was the first to use Sanderson's electronegativities to calculate the effective charge on the atoms in a zeolite structure. The calculated charges were used to correlate the physicochemical properties of the zeolite system. Of importance to the present study, the oxygen charge of Y-type zeolites was linearly related to the ionization potential of various ion-exchanged cations.

The basic strength which a zeolite exhibits has been studied by Barthomeuf and de Mallmann (*32*) using Sanderson's average electronegativities. Pyrrole adsorption on several types of zeolites, coupled with IR spectroscopy was used to measure the basicity as a function of alkali ion exchange. A decrease in the N–H stretching frequency correlated with the average electronegativity of the zeolite. The authors postulated that the pyrrole probed the more basic oxygens, thus the N–H stretching frequency would be sensitive to changes in basicity.

In at least two studies Sanderson's electronegativities have been used to interpret catalytic results. Jacobs (*33*) reported a good correlation between the average elec-

TABLE 6

Intermediate Sanderson Electronegativities and Partial Oxygen Charge for the Ru-Zeolite Catalysts

Symbol	Catalyst	S_{int}[a]	δ_O[b]
A	RuKX	3.32	−0.40
B	RuNaKX	3.44	−0.37
C	RuNaX	3.52	−0.36
D	RuKY	3.61	−0.34
E	RuCsX	3.65	−0.33
F	RuHY	4.05	−0.24
F[c]	RuHY	3.97	−0.26

[a] Intermediate Sanderson electronegativity.
[b] Partial oxygen charge.
[c] RuHY acid sites corrected for proton content (see text).

tronegativity and the TOF of isopropanol decomposition and *n*-decane hydroconversion in zeolites with high aluminum content. Of more direct interest, de Mallmann and Barthomeuf (*34*) have shown that the TOF for benzene hydrogenation in Pt-zeolites is a linear function of the average oxygen charge, as determined from the electronegativity equalization principle.

The intermediate Sanderson electronegativity (*31*, *35*) and partial oxygen charge have been calculated for the ruthenium zeolite catalysts used in this study. The values for the specific elemental compositions given in Table 1 are shown in Table 6. The Sanderson electronegativities for the significant elements are given by Mortier (*31*). The intermediate electronegativity and partial oxygen negative charge decreased upon alkali ion-exchange in the order $K^+ > Na^+ > Cs^+$. The decrease is expected between K and Na due to the difference in electronegativity; however, in general the addition of cesium should cause an increase in the calculated values. But, as noted previously, Cs^+ occupied only part of the exchange sites; the remainder were occupied by Na^+ and H^+ cations.

For a given cation, changing from an X-type to a Y-type zeolite increased the intermediate electronegativity, and the partial oxygen negative charge decreased. The trend in the values was expected due to the change in the silicon-to-aluminum ratio. The higher silicon content of the zeolite Y increases the acidity of the material which is consistent with the lower negative value of the partial oxygen charge. A problem in the H–Y zeolite was the estimation of the acid sites per unit cell. Upon correcting the number of acid sites per unit cell for the RuHY catalyst, based on results obtained by infrared spectroscopy, the calculated oxygen charge tended toward a more negative value. In the zeolites containing mainly alkali-metal cations the uncertainty in the numbers of protons was not a problem as the calculated oxygen charge was relatively insensitive to the inclusion or omission of the protons indicated in Table 1. This was the case even for the RuCsX zeolite. It is interesting to note that the increase in the O1*s* binding energy in the RuHY relative to RuKX (Table 3) is consistent with the greater amount of negative charge on the oxygens of the RuKX zeolite. The relationship between O1*s* binding energy and effective charge has been discussed by Noller *et al.* (*36*).

For the alkali-metal zeolites the turnover frequency at 350°C for ammonia synthesis appears to vary in an exponential manner with respect to the calculated partial oxygen charge, as shown graphically in Fig. 4. Thus, the variations in the type of cation and the Si/Al ratio is adequately reflected in the charge of the oxygen atoms. The deviation from the linear relationship for the RuHY catalyst, however, is quite apparent. By decreasing the number of protons from 51 to 42 per unit cell the negative charge on the oxygen increased somewhat (Table 6), but not enough to agree with the correlation. As pointed out previously, Sachtler and coworkers (*11*) have suggested that protons form adducts with the metal particles in a zeolite, and in this sense they appear to act differently than other types of cations. The present study seems to support this view. By contrast, one could also argue that the

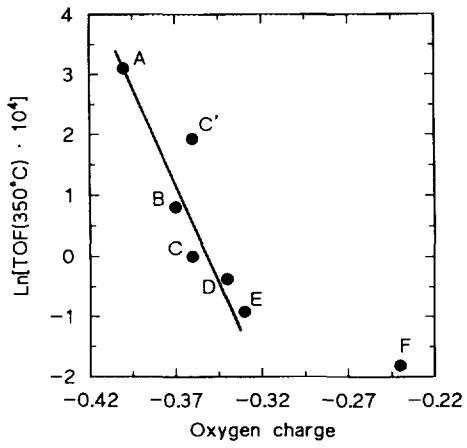

FIG. 4. Ln(turnover frequency at 350°C) versus Sanderson's partial oxygen charge: (A) RuKX, (B) RuKHX, (C) RuNaX, (C') RuNaX with 40% dispersion, (D) RuKY, (E) RuCsX, and (F) RuHY.

Sanderson electronegativity approach does not adequately take into account the uniqueness of protons as cations in a zeolite. The results of de Mallmann and Barthomeuf (*34*), however, indicate that this is not the case as their activity for a PtHY zeolite agreed nicely with the correlation established by the other zeolites.

The results for the RuNaX zeolite having a metal dispersion of 40% is plotted in Fig. 4 as datum point C'. The fact that the RuNaX zeolite with a dispersion of 90% lies below the line of Fig. 4 and the RuNaY zeolite with a dispersion of 40% lies well above the line indicates that the metal particle size is equally as important in determining the activity for ammonia synthesis as is the electronic factor introduced by the charge on the oxygen atoms. The unexpectedly large activity of the RuHY zeolite also may be a result of the larger Ru particles in this catalyst.

CONCLUSIONS

The activity of ruthenium metal particles within the cavities of faujasite-type zeolites is strongly dependent upon the type of cation present in the zeolite, the Si/Al ratio and the size of the metal particles. Of the several zeolites studied RuKX was the most active, and the TOF was observed to increase in the order $K^+ > Na^+ > Cs^+$. A RuKX zeolite was much more active than a RuKY zeolite. The effects of the alkali-metal cation and the Si/Al ratio can be adequately understood in terms of the charge on the oxygen atoms in the zeolite. As the charge becomes more negative, the TOF increases, which is consistent with the view that enhanced electron density on the metal facilitates the surface dissociation of nitrogen.

The size of the ruthenium particle is equally important as the oxygen charge. Larger particles had greater TOFs. The RuHY zeolite had an unexpectedly large TOF, considering the small amount of negative charge on its oxygen atoms, but the high TOF may in part result from the larger Ru particles in the catalyst.

When compared with the new generation of Ru-based ammonia synthesis catalysts, the TOF of the RuKX zeolite is less, but the activity per total amount of Ru is more comparable because of the large dispersion in the zeolite. The activity of the RuKX zeolite is much greater than that of a commercial Fe-based catalyst.

ACKNOWLEDGMENTS

This research was supported in part by the Regents of Texas A&M University through the AUF-sponsored Materials Science and Engineering Program. The authors are indebted to Dr. A. de Mallmann for discussions concerning the Sanderson electronegativity approach.

REFERENCES

1. Merriam, J. S., and Atwood, K. *in* "Applied Industrial Catalysis" (B. E. Leach, Ed.), Vol. 3, p. 113. Academic Press, New York, 1983.
2. Aika, K., Humio, H., and Ozaki, A., *J. Catal.* **27,** 424 (1972).
3. Ozaki, A., Aika, K., Furuta, A., and Okagami, A., U.S. Patent 3,770,658 (1973).
4. Mandelik, B. G., Cassata, J. R., Shires, P. J., and Van Dijk, C. P., U.S. Patent 4,568,530 (1986); also *Appl. Catal.* **67,** N18 (1991).
5. Aika,, K., Ohya, A., Ozaki, A., Inoue, Y., and Yasumori, I., *J. Catal.* **92,** 305 (1985).
6. Lee, S. B., Weiss, M., and Ertl, G., *Surf. Sci.* **108,** 357 (1981).

7. Larsen, G., and Haller, G. L., *Catal. Lett.* **3,** 103 (1989).
8. Gallezot, P., *Catal. Rev.-Sci. Eng.* **20,** 121 (1979).
9. Bai, X., and Sachtler, W. M. H., *Catal. Lett.* **4,** 319 (1990).
10. Ertl, G., *J. Vac. Sci. Technol. A* **1,** 1247 (1982).
11. Homeyer, S. T., Karpinski, Z., and Sachtler, W. M. H., *J. Catal.* **123,** 60 (1990).
12. Gustafson, B. L., and Lunsford, J. H., *J. Catal.* **74,** 393 (1982).
13. Elliot, D. J., and Lunsford, J. H., *J. Catal.* **57,** 11 (1979).
14. Oukaci, R., Sayari, A., and Goodwin, J. G., *J. Catal.* **102,** 126 (1986).
15. Mahdi, W., Sauerlandt, U., Wellenbüscher, J., Schütz, J., Muhler, M., Ertl, G., Schögl, R., *Catal. Lett.* **14,** 339 (1992).
16. Breck, D. W., "Zeolite Molecular Sieves." Wiley, New York, 1974.
17. Gustafson, B. L., Ph.D. dissertation, May 1981 Texas A&M University.
18. Hathaway, P. E., and Davis, M. E., *J. Catal.* **116,** 263 (1989).
19. Kuhl, G. H., and Schweizer, A. E., *J. Catal.* **38,** 469 (1975).
20. Garces, J. M., Vrieland, G. E., Bates, S. I., and Scheidt, F. M., *in* "Catalysis by Acids and Bases" (B. Imelik, Ed.), p. 67. Elsevier, Amsterdam, 1985.
21. Olson, D. H., *J. Phys. Chem.* **74,** 2758 (1970).
22. Theng, B., Vansant, E., Uytterhoeven, J. B., *Trans. Faraday Soc.* **64,** 3370 (1968).
23. Verdonck, J. J., Jacobs, P. A., Genet, M., and Poncelet, G., *J. Chem. Soc. Faraday Trans 1* **76,** 403 (1980).
24. Pedersen, L. A., and Lunsford, J. H., *J. Catal.* **61,** 39 (1980).
25. Dalla Betta, R. A., *J. Catal.* **34,** 57 (1974).
26. Oukaci, R., Sayari, A., and Goodwin, J. G., *J. Catal.* **106,** 318 (1987).
27. Okamoto, Y., Ogawa, M., Maezawa, A., and Imanaka, T., *J. Catal.* **112,** 427 (1988).
28. Hikita, T., Aika, K., and Onishi, T., *Catal. Lett.* **4,** 157 (1990).
29. Dumesic, J. A., Topsoe, H., Khammouma, M. and Boudart, M., *J. Catal.* **37,** 503 (1975).
30. Elofson, R. M., and Gadallah, F. F., U.S. Patent 4,142,993 (1979).
31. Mortier, W. J., *J. Catal.* **55,** 138 (1978).
32. Barthomeuf, D., and de Mallmann, A., *in* "Innovation in Zeolite Materials Science," (P. J. Grobet, W. J. Mortier, E. F. Vansant, and G. Schulz-Ekloff, Eds.) p. 365. Elsevier, Amsterdam, 1988.
33. Jacobs, P. A., *Catal. Rev.-Sci. Eng.* **24,** 415 (1982).
34. de Mallmann, A. and Barthomeuf, D., *J. Chim. Phys.* **87,** 535 (1990).
35. Sanderson, R. T., *Science* **114,** 670 (1951).
36. Noller, H., Lercher, J. A., and Vinek, H., *Mater. Chem. Phys.* **18,** 577 (1988).